Highly efficient TiO2 nanotubes for photocatalytic degradation reactions through optimization of textural properties

Ziba Roostaei, Frédéric Dappozze, C Guillard, Gilles Berhault

Highly Efficient TiO_2 Nanotubes for Photocatalytic Degradation Reactions through Optimization of Textural Properties

Ziba Roostaei, Frédéric Dappozze, Chantal Guillard, Gilles Berhault*

Institut de Recherches sur la Catalyse et l'Environnement (IRCELYON), CNRS – Université Lyon I, 02 avenue Albert Einstein, 69100 Villeurbanne, France

All correspondence should be sent to:

Dr. Gilles Berhault

E-mail: gilles.berhault@ircelyon.univ-lyon1.fr

Ph: (+33) 472 44 53 07

Abstract

A series of titanium dioxide nanotubes were synthesized via a hydrothermal method. By varying the preparation conditions, nanotubes with different morphologies or textural properties were produced. Various characterization techniques were used to clarify the various features of the as-prepared nanotubes. Samples with surface areas ranging between 200 and 230 m^2/g in specific surface area exhibit the maximum photocatalytic activity in the degradation of formic acid. Detailed analysis of the structural characteristics emphasizes the complex role played by surface structural defects in the tuning of their photocatalytic performance helping in this way to achieve optimal activity in photooxidation.

Keywords: catalytic; defects; hydrothermal; nanostructure; semiconducting.

1. Introduction

More than 2 billion of the world's population do not have access to clean water resources. 42.2% of this population drinks contaminated water without appropriate sanitation. According to different studies, industrial activities and discharge areas are the major reasons for water contamination.[1]

In the last years, photocatalysts have been more and more considered as promising materials for water treatment.[1,2] However, in most cases, photocatalysts are active only under UV light which builds up only a slight fraction of the solar spectrum, around 5%. In addition, there is always a high probability for the recombination of the electron-hole pairs. This phenomenon limits the effectiveness of photocatalysts. Thus, the attention of many research studies has been paid to limit the recombination of photogenerated charges in heterogeneous photocatalysts.[3]

TiO_2 as the most known photocatalyst can be used in a variety of applications for wastewater treatment due to its fascinating properties. In strong contrast to other semiconductors, TiO_2 is stable under various environments (acid, basic). It is also known to be the most photoactive semiconductor under UV light. The position of its energy bands gives it a strong oxidizing/reducing power when excited under UV radiation.[4,5] In addition, thermal stability, low price, eco-friendly properties, and energy conversion are some other fascinating features of titanium dioxide that have made it favored compared to other photocatalysts in the last recent years.[6]

However, TiO_2 shows two main drawbacks: a too high propensity for electron-hole recombination and an inability to work under visible illumination. To solve these drawbacks, two options have been envisaged. The first one is based on the extension of the wavelength domain for which TiO_2 can be excited to the visible light range (i.e. decreasing band gap). The second strategy is to limit the probability of the recombination of e^-/h^+ pairs. Generally, different methods such as the preparation of co-catalysts or composites using precious metals, various photocatalysts, doping, adjusting the structure of photocatalysts, etc. are considered effective procedures to increase the productivity of photocatalysts.[7-9]

Controversial results have been reported about the role of various properties of semiconductors including morphology, particle size, crystallite size, etc. on their photocatalytic performance. For instance, particle size is often regarded as the most important factor for reactivity. However, Wu et al. have recently shown a complex role of particle size in relation to the propensity of a given semiconductor to form surface or bulk defects, bulk defects playing a negative role by favoring electron-hole recombination for particles larger than 10 nm.[10] In addition, crystallite

size and morphology were also found to influence the photocatalytic, optical, and electrical characteristics of semiconductors. In this respect, while Song et al. showed a beneficial effect of a nanotubular morphology in Rhodamine B photodegradation,[11] other authors observed mainly a beneficial role of surface area but only on TiO_2 thin films.[12] However, this approach remains oversimplistic. Indeed, one should not ignore that the BET specific surface area is not a parameter varying independently from the crystallite size and/or the morphology, all these factors being interdependent.

In comparison with many conventional materials, the characteristics of titanium dioxide nanostructures can vary depending on their morphologies and sizes.[5] In this respect, Turki et al. observed that a large specific surface area combined with a low crystallite size leads to an optimization in the photocatalytic performance of titanium dioxide nanotubes.[13] In 1996, Hoyer reported the fabrication of titanium dioxide in nanotubular form for the first time. He used the electrochemical deposition method in a porous aluminum oxide matrix.[14] Then, a hydrothermal process was developed by Kasuga et al. allowing the production of TiO_2 nanostructures in large quantities at reasonable cost in 1998.[15] Hydrothermal process, compared to other methods such as the template approach or the anodic oxidation, is an inexpensive and easy to implement process, to produce TiO_2 nanotubes in large amount.[13]

The hydrothermal treatment is generally carried out in a strongly basic medium at a controlled temperature and pressure. After being initially developed by Kasuga et al.,[15] the alkaline hydrothermal method for the production of TiO_2 nanotubes has been optimized by different research groups. For instance, tetrabutyl orthotitanate has been one of the basic materials that has been used to produce nanorods of titanium dioxide.[16] According to previous work in our research group,[13] the $Na_2Ti_2O_5.H_2O$ nanotubes formation is summarized as:

$$2\ TiO_2 + 2\ NaOH \rightarrow Na_2Ti_2O_5.H_2O$$

When the pH is acidified, an ion exchange between H^+ and Na^+ occurs:

$$Na_2Ti_2O_5.H_2O + x\ H^+ \leftrightarrow Na_{2-x}H_xTi_2O_5.H_2O + x\ Na^+ \quad (0 \leq x \leq 2)$$

$Na_2Ti_2O_5.H_2O$ nanotubes can therefore be totally transformed to $H_2Ti_2O_5.H_2O$ (hydrogenotitanate nanotubes) with an orthorhombic phase.

In the present study, nanotubes were synthesized using an alkaline hydrothermal method based on previous studies in our research group.[17] In order to better analyze the role of textural properties, and in particular of the specific surface area on the photocatalytic activity of the system of interest here (TiO_2 nanotubes), a systematic evaluation of the influence of the specific surface area (and therefore of the crystallinity) of our materials was herein carried out for the

photocatalytic degradation of formic acid used as a representative model molecule illustrating the degradation of molecules containing carboxylic groups.

It should be noted first that the effect of the NaOH concentration used and or of the hydrothermal temperature were already studied in a previous work.[17] Similarly, the effect of the calcination step was also evaluated.[13] However, even when controlling precisely the NaOH concentration used or the hydrothermal temperature, some variabilities can still be observed mainly on the final textural properties. Therefore, other parameters influencing the crystallite size and the BET surface area were systematically varied: 1) duration time after the hydrothermal treatment for which the samples remain in the presence of NaOH, 2) the temperature used during the washing steps with hot water after the neutralization with HCl (vide infra) and finally 3) the rate at which these latter washing steps was performed. These parameters were selected since known to affect each of the two main steps leading to the formation of nanotubes: 1) the hydrolysis rate leading to the breaking of Ti-O-Ti bonds and the formation of intermediate titanate layers intercalated by sodium ions [13] for the case of the time left with NaOH or 2) the removal of sodium destabilizing these layers and inducing their rolling into multiwalled nanotubes for the temperature or the rate applied for the washing steps.[13] Finally, this study will also be performed by comparison to a classical TiO_2 P25 reference.

2. Materials and Methods

2.1. Chemicals

Nanotubes were produced using a commercial titanium dioxide (P25- 72% anatase/28% rutile, Evonik) as the starting material. Other ingredients included NaOH (Carlo Erba Reagents), HCl 30 vol % (Fluka), formic acid (98% purity, Sigma Aldrich), and ultra-pure water (18 $M\Omega.cm^{-1}$).

2.2. Synthesis of TiO_2 Nanotubes (NTs)

TiO_2 nanotubes were prepared using the alkaline hydrothermal route that has been employed in previous studies in our research group.[13] This alkaline hydrothermal method contains four main steps. First, a strong alkaline NaOH solution (11.25 M) was prepared and 3 g of commercial P25 was dissolved in 90 mL of this solution for 5 minutes under stirring. This solution was then transferred to a 200 mL Teflon container placed inside a stainless-steel

autoclave. Afterwards, the resulting solution was treated via a hydrothermal process at 130°C for 20 h in a programmed oven with a temperature rate of 2 °C.min^{-1}.

In the second step, after the hydrothermal process, the obtained material was washed and vacuum filtered using 4 L of hot distilled water (18 MΩ.cm^{-1}) to remove the NaOH in excess (the pH would be 10.2 after this washing step) using a Buchner glass filter of porosity of 3 (16-40 µm). The solid was then gradually neutralized with 0.1 M HCl solution to a pH of nearly 6.6. The neutralization step leads to an exchange between Na^+ and H^+ ions with formation of sodium chloride. This sample was then washed again using 2 L of hot distilled water (18 MΩ.cm^{-1}) to remove the NaCl present in the material and the remained solid was then transferred to an oven to be dried at 80° C for 20 h under air.

In the third step, the dried solid (3.5 g) was crushed and dissolved in 175 mL of a more concentrated solution of HCl (1 M) for 30 min in order to eliminate the residual sodium, then washed using 1 L of hot distilled water. The washing process with HCl and water should be performed twice during this step. In the final hot-water washing step, pH equals to 7. The final material was then separated from the filter and dried in an oven at 80° C for 20 h under air to obtain the nanotubes in a hydrogenotitanate phase ($H_2Ti_2O_5.H_2O$).

In the fourth step, a thermal treatment (Figure 3) was carried out under air at 400°C for 2 h with a heating rate of 2°C/min and an air flow rate of 10 mL/min to convert the hydrogenotitanate phase into anatase while keeping the nanotubular morphology. The final weight of the product at this step is approximately 2.5 g. The morphology of the nanotubes can be affected by various factors such as the precursor used (anatase, rutile, or amorphous), the basic solution, the hydrothermal process, the washing and calcination steps.

2.3.Photocatalytic degradation of formic acid

TiO_2 nanotubes were used in the photocatalytic degradation process of formic acid in an aqueous solution. Formic acid has been chosen as the simplest carboxylic acid with only one final product of degradation, carbon dioxide, therefore without any complicated by-products during the mineralization process. Moreover, formic acid is often the last intermediate in the degradation of a large family of pollutants based on carboxylic acids and is therefore representative of the last step leading to complete mineralization into CO_2 and H_2O.

30 mg of each photocatalyst was added to 30 mL of formic acid (1 g/L) in the aqueous phase (C = 50 ppm) in a 100 mL Pyrex reactor, open to air under magnetic stirring at 450 rpm. The pH value of formic acid was determined to be nearly 3.5. The optic window of the Pyrex

photoreactor at the bottom part (12.5 cm^2) is exposed to the light source and used to transfer the light to the suspension. The solution of formic acid and photocatalyst remains in the dark for half an hour under stirring to obtain an equilibrium between the adsorption and desorption of formic acid on the surface of the photocatalyst. Then it was irradiated with UV light using a Philips PLL 18 W low-pressure mercury lamp centered at 365 nm (UVA). The distance of the optical window from the source of UV light was fixed to receive the same intensity of irradiation during all experiments (2.8 mW/min). This value was measured by means of a VLX-3W radiometer supplied with a CX-365 detector (UVA). The UV lamp was turned on 15 minutes before every degradation test under irradiation to be stabilized and to emit the same number of photons.

Problems coming from in situ heating due to irradiation was not observed since the degradation time of formic acid was short. The initial concentration of formic acid before any degradation was determined as C_0. Samples at time zero and after 2 minutes intervals (until 10) were taken by means of a 1 mL syringe (the required quantity was 0.5 mL). The solid photocatalyst was then separated from the liquid part using Nylon syringe filters with 0.45 μm pore size. All the liquid samples obtained after filtration were then analyzed using a High-Performance Liquid Chromatography (HPLC) equipment.

2.4. Characterizations

Sodium values were first measured by inductively coupled plasma optical emission spectroscopy (ICP-OES) technique applying an Horiba Jobin Yvon Activa analyzer.

X-ray Diffraction (XRD) was conducted utilizing a Bruker D8 Advance AXS diffractometer equipped with a Cu Kα source (λ = 1.54184 A˚) and a LynxEye detector. Analysis conditions were performed in a 2θ scale range between 4 and 80º with a 0.02° scan rate and a 96 s dwelling time. Operation voltage was fixed at 40 kV and current at 100 mA. Diffrac.EVA program was used to specify the phases from the ICDD-PDF4+ database. The Debye-Scherrer formula was applied to determine crystallite sizes in the various samples. This formula is applied for powders with crystallite sizes up to 100 nm as follows in equation (1).

$$L = K\lambda/\beta\cos\theta \qquad (1)$$

In this equation, L is considered as the crystallite size, K is the shape factor (equal to 1.0 for nanotubes and 0.9 for P25), λ and β being respectively the X-ray wavelength, and the full width at half maximum.

The BET specific surface area of the synthesized nanotubes was measured using a Micromeritics ASAP 2020 instrument. The samples were first degassed at 300° C for 3 h under vacuum. Then, nitrogen adsorption-desorption measurements were performed at -196° C in a relative pressure range from 0.05 to 0.25. Pore size distribution using the Barrett–Joyner–Halenda (BJH) method were also determined considering the desorption branch of the isotherms.

Raman spectra of the different samples were acquired on a LabRAM-HR appliance from Horiba. All spectra were recorded from 50 to 1000 cm^{-1} with a 4.0 cm^{-1} spectral resolution, and a 532 nm Ar-Kr RM2018 laser at room temperature. The irradiating power was fixed at 550 µW.

UV-vis spectra were obtained using an AvaSpec-2048 Fiber Optic Spectrometer equipped with a 2048-pixel CCD detector array. Barium sulfate was used as a reference and all data were measured in the 200-800 nm wavelength range. Subsequently, band gaps were calculated based on the Kubelka–Munk formula.

Transmission Electron Microscopy (TEM) was performed using a JEOL 2010 microscope operating at 200–400 kV in order to analyze the surface morphology of the nanotubes. The prepared solutions containing nanotubes were dried on a carbon film set on a Cu grid (300 mesh), then analyzed using an ultrahigh-resolution (1.9 A˚) polar piece.

3. Results and Discussion

3.1. ICP Results

In an initial work, Guillard et al.[18] observed that sodium salts such as NaCl can decline the efficiency of TiO_2 photocatalysts for the degradation of methylene blue. Similar observations were observed on TiO_2 nanotubes if sodium is not enough removed after the hydrothermal treatment during washing steps with HCl.[13] Therefore, before any other characterization, in a first step, all our nine TiO_2 samples were submitted to inductively coupled plasma - optical emission spectroscopy (ICP-OES) analysis to determine the amount of residual sodium after the washing steps performed after the hydrothermal treatment. Results are reported in Table 1. In almost all cases, only 0.01 wt% of Na was detected which is considered to be too low to significantly affect the photocatalytic response confirming in this way previous studies.[13]

3.2. N_2 Adsorption-Desorption Measurements

The BET specific surface areas of the various samples of titanium dioxide nanotubes were determined by N_2 adsorption-desorption measurements at -196°C in the relative P/P_0 pressure range between 0.05 and 0.25. The different TiO_2 nanotubes obtained present specific surface areas ranging between 160 and 285 m^2/g (Table 1) and will be labelled afterwards NT-X with X the specific surface area in m^2/g.

In a first step, reproducibility was checked by performing six successive syntheses using the same conditions for preparation: pH of neutralization = 6.6-6.7, residence time left in NaOH: 18 h, temperature (60°C) and a high rate (3 L/h) for the washing steps (Table 1). Results show a high rate of reproducibility in terms of specific surface areas with values going from 200 to 226 m^2/g (average value: 211 m^2/g). Considering that systematic errors for S_{BET} values determination is about ± 5 %, results show a quite good homogeneity in terms of textural properties.

In a second step, the influence on textural properties of some preparation conditions such as the time left with NaOH after the hydrothermal treatment, the temperature for the washing steps with hot water as well as the rate at which the washing treatment was performed were evaluated (Table 1). In this respect, the sample with the lowest S_{BET} value (160 m^2/g) was found when a low rate for the washing steps was used. On the other hand, the sample with the highest S_{BET} of 285 m^2/g is synthesized when washed with hot ultra-pure water at 80 °C instead of 60°C. Finally, TiO_2 nanotubes with a BET surface area of 253 m^2/g was obtained if the time left with NaOH at the end of the hydrothermal treatment was increased to 24 h instead of 18 h (average value in this case: 211 m^2/g).

N_2 adsorption-desorption isotherms were more deeply analyzed considering both types of isotherms and of hysteresis loops. As shown in Figure 1A, all the different TiO_2 samples exhibit type IV isotherms based on the IUPAC classification. Interestingly, the hysteresis loops change of shapes with the specific surface area of the different TiO_2 samples. In the case of NT-160, the hysteresis loop is quite close to type H3 and corresponds to an intergranular porosity which is not associated to any defined mesoporosity. For NT-211 and NT-285, the hysteresis loops result more from the combination of H1 and H3 types revealing in this case the supplementary presence of mesopores. However, one should note here that this mesoporosity only results from an intergranular porosity formed by the aggregation of bunched TiO_2 nanotubes as typically observed on TEM images.[19] A slight shift of the onset value for P/P_0 can also be noticed for NT-285 suggesting the formation of smaller pores in this case. Finally, for NT-253, the

hysteresis loop still shows a combination of H1 and H3 types but with a higher proportion of H3 suggesting a lower proportion of mesopores due to intergranular porosity of nanotubes, and therefore a lower proportion in nanotubes or a more disorganized nanotubular morphology.

The determination of the pore size distributions using the BJH method has also been determined and results are reported in Figure 1B. Similarly, values for pore diameters and porous volumes are given in Table S1. First of all, as explained before, the porosity measured here corresponds mainly to the void space created between agglomerated TiO_2 particles (mainly nanotubes) and therefore it does not reflect any real intrinsic mesoporosity of the materials. Porous volumes shown in Table S1 should then be considered cautiously. Nevertheless, some interesting points can still be noted for the pore size distributions reported in Figure 1B. First, as shown in the inset, a shoulder around 3.5 nm can be noticed in all samples corresponding to the inner porosity of the TiO_2 nanotubes. Moreover, net differences in the pore size distributions of the four samples reported in Figure 1B can be observed. For NT-160, only a broad low intense distribution can be noted accompanied by a shoulder shifted to lower values (about 3.0 nm) suggesting that if nanotubes are formed, their 1D morphology should be less developed. A high degree of shape heterogeneity therefore remains present leading to a large undefined distribution resulting from void spaces between particles. For NT-211 and NT-285, similar sharp and intense distributions can be noted suggesting the formation of nanotubes with similar dimensions and inner diameters leading to similar void spaces. Finally, for NT-253, the distribution appears broader while the maximum shifts to higher values. This indicates that increasing the time left with NaOH after the hydrothermal treatment from 18 to 24 h leads to a more heterogeneous distribution but with similar inner diameters for the TiO_2 nanotubes.

3.3. X-ray Diffraction

XRD analysis of the various TiO_2 samples was also performed and the resulting diffractograms are reported in Figure S1. All diffraction patterns exhibit typical peaks characteristic of the anatase phase (JCPDS n° 21-1271) with main contributions at 2θ values of 25.3°, 38.0°, 48.0°, 54.0°, 55.0° and 62.6° corresponding respectively to the (101), (004), (200), (105), (211) and (204) reflections.[13] Moreover, an additional low intense contribution around $2\theta \sim 15°$ can be noticed in all samples except for NT-160 which corresponds to the interlayer distance between walls of the nanotubes.[20] Therefore, the observation made here suggests that TiO_2 nanotubes have not been formed (at least in a significant proportion) in the case of NT-160.

The Debye- Scherrer equation was therefore utilized to measure the crystallite sizes considering the full width at half maximum (FWHM) of the (101) peak of anatase. Table 1 reports the evolution of the crystallite sizes of anatase for the different samples. The NT-160 material, for which a low rate was applied for the washing steps, also presents the highest value of crystallite size (11.8 nm). For all the samples presenting S_{BET} values between 200 and 226 m^2/g, the crystallite sizes remain essentially similar with values ranging between 8.7 and 9.2 nm. This once again indicates a high degree of reproducibility in the preparation of TiO_2 nanotubes allowing a good control of textural properties. Increasing further the surface area to 253 m^2/g and then to 285 m^2/g results in a progressive and net decrease of the crystallite size first to 8.0 nm and then to 6.5 nm. This loss in crystallinity could be related to the concomitant formation of bulk structural defects limiting crystalline domain sizes.

3.4. Raman Spectroscopy

Structural properties were also determined using Raman spectroscopy for the different TiO_2 samples with various S_{BET} specific surface areas (Figure 2A). In all samples, five main vibrational bands at ~ 143 cm^{-1} (E_g), 195 cm^{-1} (E_g), 391 cm^{-1} (B_{1g}), 513 cm^{-1} (B_{1g}/A_{1g}) and 635 cm^{-1} (E_g) can be attributed to the anatase phase.[21] In addition, in all the samples except NT-160, several additional minor contributions can be detected between 200 and 300 cm^{-1}. These bands, observed at 238, 253, and 287 cm^{-1}, are assigned to the TiO_2(B) phase.[22] Other TiO_2(B) bands expected at 123, 145, 172, 196, 365, 400, and 478 cm^{-1} cannot be observed since overlapping with anatase contributions.[13] Moreover, the NT-160 sample does not show these TiO_2(B) additional contributions. Results acquired previously have shown that during the process for TiO_2 nanotube formation, the hydrogenotitanate phase observed before calcination first converts to an intermediate TiO_2(B) phase before obtaining the final anatase phase.[13] In the case of NT-160, the absence of the TiO_2(B) phase suggests a direct transformation from the hydrogenotitanate phase to anatase.

A deeper analysis was then performed considering the main E_{1g} vibrational mode giving rise to an intense signal around 143 cm^{-1}. Indeed, increasing the specific surface area leads to a systematic shift to higher wavenumbers of this band going from 141.5 cm^{-1} for NT-160 to 143.4 cm^{-1} for NT-211, 143.9 cm^{-1} for NT-226, 144.1 cm^{-1} for NT-253 and finally 144.9 cm^{-1} for NT-285. This important shift of 3.4 cm^{-1} on the whole range of specific surface areas obtained indicates a continuous and important creation of structural defects at the surface of anatase.[23]

According to the shifts observed, one main specific surface area region where the number of defects would increase the most is when passing from NT-253 to NT-285. This corresponds to the samples presenting a net decrease in crystallite sizes as observed previously by XRD. These results suggest that two main regions can be distinguished according to their respective Raman shifts and XRD crystallite size changes. In a first step, for S_{BET} surface areas values around 200-230 m^2/g, only surface structural defects were formed characterized by moderate shifts in Raman and no variation in crystallite sizes. However, above 230 m^2/g, more significant Raman shifts were found accompanied by a net decrease in XRD crystallite sizes suggesting the formation in this latter case of more deep structural defects.

3.5. UV-vis Spectroscopy

Apart from the structural properties, optical features are also important parameters that should be surveyed. UV-vis spectra of the different TiO_2 samples are shown in Figure S2. All the different samples present very similar spectra with a strong absorption region below 400 nm due to $O^{2-}(2p) \rightarrow Ti^{4+}(3d)$ charge transfer processes. One should however note for NT-211 and other samples with higher surface areas a higher contribution in the absorbance zone around 300-350 nm than for P25 or NT-160. This higher contribution could be related to the appearance of structural defects.[24, 25] Moreover, similar onset values are observed in all cases showing that the modification of textural and morphological properties does not influence significantly the optical characteristics of our materials. This fact was confirmed through the calculation of the band gap energy (E_g) values using the Kubelka-Munk methodology and assuming an indirect band gap transition as expected for anatase. Band gap E_g results are reported in Table S2 for all our samples and for P25 for comparison purposes. In all cases, band gap values were measured in a similar range going from 3.16 eV to 3.30 eV without clear evolution whatever the samples considered. These results clearly emphasize the absence of any major influence of textural and/or morphological properties on the optical features of our materials even if formation of some structural defects can marginally affect the absorbance in the 300-350 nm region.

3.6.Transmission Electron Microscopy

The morphology and dimensions of the synthesized nanotubes were also analyzed using transmission electron microscopy. In the TEM results presented in Figure 2B, the stacked and agglomerated nanotubular structures are evident for three of the samples: NT-211, NT-253, and

NT-285. Large agglomeration of TiO_2 nanotubes is commonly observed on TEM images of these 1D materials. It results from important Van der Waals forces between nanotubes leading to their agglomeration when preparing grids for TEM visualization following the deposition of drops of their suspension.[13]

This agglomeration makes the exact measurement of the length of these nanotubes quite difficult even if this length should be of several hundreds of nm. The inner diameter of these nanotubes can also be directly evaluated from the TEM images particularly for NT-253 and NT-285. In the case of NT-253, the inner diameter appears to be around 6 nm while the outer diameter reaches 12 nm leading to a wall thickness of around 3 nm in agreement with values found previously.[13] For NT-285, the inner diameter slightly decreases to 5 nm while the wall thickness remains essentially unchanged, around 3 nm. Even if less clearly visible by TEM on NT-211, the inner diameter seems to be maintained around 6 nm. Looking at Table 1, this suggests that increasing the residence time in the presence of NaOH after the hydrothermal treatment from 18 h to 24 h does not influence the internal porosity of the nanotubes while on the opposite, accelerating the elimination of sodium through the use of a higher temperature for the washing steps induces some shrinking of the internal porosity of our materials.

This last result can be understood considering the mechanism leading to the enrolment of TiO_6 sheets initially stabilized by intercalated sodium ions. The elimination of sodium ions is known to destabilize the lamellar sheets leading to the rolling of these nanosheets into nanotubes to remove dangling bonds.[15] In this case, accelerating the elimination of sodium ions should also lead to an acceleration of the rolling process forming multi-walled nanotubes and the formation of narrower inner diameters.

One particular case corresponds to NT-160 (Figure 2Ba). In this last case, only few nanotubes with bigger diameters can be noticed while other non-defined particles can also be observed. This result confirms previous observations made by N_2 adsorption-desorption measurements, XRD and indirectly Raman. First of all, N_2 adsorption-desorption isotherms as well as BJH pore size distributions emphasized the complete different textural properties of NT-160 with a lack of mesoporosity and the absence of intergranular porosity due to the agglomeration of nanotubes even if some intragranular porosity can still be detected. This confirms also XRD analyses which show the absence of a 2θ contribution at around 14° due to the interlayer distance characteristic of nanotube walls. Finally, the non-detection of TiO_2(B) on the Raman spectrum of NT-160 also suggests a different transformation from hydrogenotitanate to the anatase phase during calcination. This indeed differs from the commonly observed formation of the intermediate TiO_2(B) phase for nanotubular samples. The absence or low amount of

nanotubular structures for NT-160 is related to the rate at which the washing steps were done. Slowing down the speed for washing means a longer time (3 h instead of 1 h) to perform these steps and therefore a longer time passed by the sample to stay in the presence of residual HCl coming from the neutralization step performed before the washing steps. This emphasizes the inherent low stability of the nanotubular morphology under moderately strong acidic conditions.[26]

3.7. Photocatalytic Activity in Formic Acid Photodegradation

The photocatalytic performance experiments of P25 and the synthesized TiO_2 nanotubes were conducted under identical conditions. The photocatalytic degradation of formic acid (50 ppm) using 1g/L of TiO_2 and under UVA light (2.8 mW/cm^2) was investigated. First, the suspension of photocatalyst/formic acid was kept in the dark for 30 min to achieve adsorption-desorption equilibrium conditions for formic acid at the surface of the TiO_2 samples. The UVA lamp was pre-heated for 15 min to reach stabilized conditions before each test. After 30 min in the dark, sampling was performed every 2 min. The photodegradation performances are exhibited in Figure S3.

All samples show a rapid linear decrease in the concentration of formic acid with the reaction time with complete degradation obtained after 16-17 minutes for the best photocatalysts. It should be noted here that only initial degradation rates will be provided since in our conditions, first-order kinetics can only be reached at concentrations in formic acid lower than 50 ppm for which photodegradation is so rapid that not sufficient experimental points for determining rate constant values can be acquired. Looking at Figure S3, significant differences in photocatalytic activity can be noticed. P25 exhibits the lowest photocatalytic activity for the degradation of formic acid. On the opposite, increasing the S_{BET} surface area from 160 to 211 m^2/g leads to a significant increase in photocatalytic activity with the highest initial degradation rate achieved for NT-211. Increasing further the S_{BET} surface area leads to a progressive decrease of the photocatalytic performance for NT-253 while NT-285 goes back to the same level in photoactivity than P25.

The initial rates of reaction (r_0) are reported in Table 2. This table also reports conversion values after 10 min of reaction as well as the time necessary to achieve full conversion. Results confirm the optimum achieved in the photocatalytic degradation of formic acid for NT samples presenting surface areas ranging between 200 and 226 m^2/g showing also the high reproducibility achieved in the synthesis and photocatalytic performances of TiO_2 nanotubes.

Optimized formation of TiO_2 nanotubes allows obtaining photocatalytic activity twice more active than the P25 reference showing a S_{BET} value of 50 m^2/g (r_0 =1.45 ppm/min). Another interesting point can be observed when comparing NT-160 formed mainly of non-1D particles to the TiO_2 nanotubes showing the optimum in activity. Indeed, in this case, one should observe a proportional relationship between BET specific surface areas and initial rates of degradation (S_{BET} NT-200/S_{BET} NT-160 ~ r_0 NT-200/r_0 NT-160). This interesting result clearly emphasizes here an apparent correlation between the increase in surface area and a resulting increase in activity and that independently of the fact that a nanotubular morphology is achieved or not. This confirms previous studies that show a direct relationship between the photocatalytic performance in formic acid degradation and the amount of formic acid adsorbed.[13] The main interest of a nanotubular morphology would be to achieve high surface areas and therefore high accessibility to the reactant. This last conclusion should however be moderated when considering anatase crystallite sizes as determined by XRD as well as Raman results about the formation of structural defects like surface oxygen vacancies. Indeed, as shown before, going from NT-160 to NT-200 leads to a decrease in crystallite sizes from 11.8 to 9.2 nm suggesting that the increase in surface area observed here is also accompanied by a higher formation of structural defects, as confirmed by Raman spectroscopy.

Increasing the S_{BET} surface area above 230 m^2/g leads to a progressive loss in photocatalytic activity with NT-285 going back to a level of activity similar to P25 (Table 2). As suggested before, the main reason behind such a loss in performance can be related to a decrease in crystallite sizes (and concomitantly the formation of bulk instead of surface structural defects) when going from NT-226 to NT-253 and finally NT-285 with values decreasing respectively from 8.7 to 8.0 and finally 6.5 nm showing once again a direct link between increase in surface area, decrease in crystallinity and formation of bulk structural defects.

Results acquired here therefore emphasize the complex role played by structural defects whose role can shift from positive to negative according to the proportion of them formed at the surface of the semiconductor and their location at the surface or more inside the bulk of the material. While a formation of those species in the surface of the semiconductor appears to play a positive role by capturing photoelectrons leaving holes available for photooxidation, as already observed by Meksi et al.,[23] a too high formation of those species by creating new defects more inside the bulk of the material alters negatively the performance of the resulting TiO_2 semiconductor through probably the formation of trap states inside the band gap favoring electron-hole recombination phenomenon.

It is worth noting that in this study, two commercial TiO_2 in the anatase phase including UV100 (S_{BET} 300 m^2/g) and HPX-200/v2 (S_{BET} 96 m^2/g) with nanosphere structure were also tested in the degradation of formic acid in the same conditions as for the nanotubes.[27] The results acquired for these materials are compared in Figure S4 with our anatase nanotubular samples with different BET surface areas and confirm that variation in the surface area and therefore of structural defects plays here a more important role compared to morphology.

The complex role played by surface area was exemplified by several previous studies using TiO_2 photocatalytic systems. Singh et al.[28] observed a higher activity with an increase in surface area and a decrease in crystallite sizes in contradiction with our results. However, the marginal increase in surface area and decrease in crystallite sizes observed in this last study makes their assignment inconclusive. Sahrin et al.[29] observed on the opposite a clear effect between higher photocatalytic performance and higher crystallinity and fewer defects. Similarly, Zhang et al.[30] studied the influence of crystallinity on the photoactivity of molybdenum-doped anatase/rutile TiO_2 nanotubes. They observed that a higher crystallinity leads to lower defects which increased the degree of photoconversion. Our results therefore allow to exemplify the fact that such conclusions were oversimplistic and that the creation of structural defects can play an ambivalent role which depends on the amount of those species formed and their precise location on or inside the material.

4. Conclusion

In this study, the influence of several preparation conditions on the structural, optical, morphological and photocatalytic properties of TiO_2 samples synthesized by the hydrothermal route under strong alkaline conditions was examined. Three synthesis parameters were evaluated in a systematic way: the residence time left with NaOH after the hydrothermal treatment, the temperature used for the washing steps after the synthesis and neutralization by HCl and finally the rate at which these washing steps are performed. Results first confirm that in all cases, anatase samples were obtained with similar optical properties. Increasing the residence time left with NaOH from 18 to 24 h or the temperature for the washing steps from 60°C to 80°C leads in both cases to an important increase in surface area, even more important in the case of the temperature for the washing steps, but without altering the nanotubular morphology. On the opposite, slowing the rate at which the washing steps is done leads to a significant loss in surface area and of the nanotubular morphology. In this last case, this result emphasizes the inherent fragility of TiO_2 nanotubes in the presence of moderately strong acidic

conditions as those prevailing here following the presence of residual HCl coming from the neutralization step performed with HCl and preceding the washing steps with hot water.

The passage from a non-defined morphology for NT-160 to well-defined TiO_2 nanotubes for NT-200 and other samples with higher surface area is accompanied by a significant increase in photocatalytic activity which can be correlated to an increase in surface area.

Increasing the surface area above 230 m^2/g leads to a loss in crystallinity as well as a too high formation of structural defects which negatively impacts the activity of TiO_2 nanotubes. This last point highlights the complex role played by structural defects on the ability of the TiO_2 semiconductor to perform efficiently photocatalytic reactions.

Acknowledgements

Z. Roostaei thanks Campus France and Région Auvergne Rhöne-Alpes for his scholarship.

Declarations

Conflict of Interest

On behalf of all authors, the corresponding author states that there is no conflict of interest.

References

1. V. Subhiksha, S. Kokilavani, S. Sudheer Khan, Recent advances in degradation of organic pollutant in aqueous solutions using bismuth based photocatalysts: A review. Chemosphere **290,** 133228 (2022).

2. N.A. Mohd Razali, W.N. Wan Salleh, F. Aziz, L.W. Jye, N. Yusof, A.F. Ismail, Review on tungsten trioxide as a photocatalysts for degradation of recalcitrant pollutants. J. Clean. Prod. **309,** 127438 (2021).

3. A. Sharma, P. Negi, R.J. Konwar, H. Kumar, Y. Verma, Shailja, P.C. Sati, B. Rajyaguru, H. Dadhich, N.A. Shah, P.S. Solanki, Tailoring of structural, optical and electrical properties of anatase TiO_2 via doping of cobalt and nitrogen ions. J. Mater. Sci. Technol. **111**, 287–297 (2022).

4. Z. Li, S. Wang, J. Wu, W. Zhou, Recent progress in defective TiO_2 photocatalysts for energy and environmental applications. Renew. Sustain. Energy Rev. **156,** 111980 (2022).

5. T. Gupta, Samriti, J. Cho, J. Prakash, Hydrothermal synthesis of TiO_2 nanorods: formation chemistry, growth mechanism, and tailoring of surface properties for photocatalytic activities. Mater. Today Chem. **20**, 100428 (2021).

6. M.M. Abutalib, H.M. Alghamdi, A. Rajeh, O. Nur, A.M. Hezma, M.A. Mannaa, $Fe_3O_4/Co_3O_4–TiO_2$ S-scheme photocatalyst for degradation of organic pollutants and H_2 production under natural sunlight. J. Mater. Res. Technol. **20**, 1043–1056 (2022).

7. T. Su, Z.D. Hood, M. Naguib, L. Bai, S. Luo, C.M. Rouleau, I.N. Ivanov, H. Ji, Z. Qin, Z. Wu, Monolayer $Ti_3C_2T_x$ as an Effective Co-catalyst for Enhanced Photocatalytic Hydrogen Production over TiO_2. ACS Appl. Energy Mater. **2**, 4640–4651 (2019).

8. Y. Chen, W. Gu, L. Tan, Z. Ao, T. An, S. Wang, Photocatalytic H_2O_2 production using Ti_3C_2 MXene as a non-noble metal cocatalyst. Appl. Catal. A Gen. **618**, 118127 (2021).

9. H. Wang, R. Peng, Z.D. Hood, M. Naguib, S.P. Adhikari, Z. Wu, Titania Composites with 2D Transition Metal Carbides as Photocatalysts for Hydrogen Production under Visible-Light Irradiation. ChemSusChem. **9,** 1490–1497 (2016).

10. Z.J. Wu, S. Cao, C. Zhang, L.Y. Piao, Effects of Bulk and Surface Defects on the Photocatalytic Performance of Size-Controlled TiO_2 Nanoparticles. Nanotechnology **28**, 275706 (2017).

11. H. Song, K. Cheng, H.F. Guo, F. Wang, J.L. Wang, N.F. Zhu, M.X. Bai, X.Q. Wang, Effect of Ethylene Glycol Concentration on the Morphology and Catalytic Properties of TiO_2 Nanotubes. Catal. Comm. **97**, 23-26 (2017).

12. B. Henkel, A. Vahl, O.C. Aktas, T. Strunskus, F. Faupel, Self-Organized Nanocrack Networks: a Pathway to Enlarge Catalytic Surface Area in Sputtered Ceramic Thin Films, Showcased for Photocatalytic TiO_2. Nanotechnology **29**, 035703 (2018).

13. A. Turki, H. Kochkar, C. Guillard, G. Berhault, A. Ghorbel, Effect of Na content and thermal treatment of titanate nanotubes on the photocatalytic degradation of formic acid. Appl. Catal. B Environ. **138–139,** 401–415 (2013).

14. P. Hoyer, Semiconductor nanotube formation by a two-step template process. Adv. Mater. **8,** 857 (1996).

15. T. Kasuga, M. Hiramatsu, A. Hoson, T. Sekino, K. Niihara, Formation of titanium oxide nanotube. Langmuir **14**, 3160–3163 (1998).

16. I.F. Mironyuk, L.M. Soltys, T.R. Tatarchuk, K.O. Savka, Methods of titanium dioxide synthesis. Phys. Chem. Solid State **21**, 462–477 (2020).

17. H. Kochkar, N. Lakhdar, G. Berhault, M. Bausach, A. Ghorbel, Optimization of the Alkaline Hydrothermal Route to Titanate Nanotubes by a Doehlert Matrix Experience Design. J. Phys. Chem. C **113,** 1672-1679 (2009).

18. C. Guillard, E. Puzenat, H. Lachheb, A. Houas, J.M. Herrmann, Why inorganic salts decrease the TiO_2 photocatalytic efficiency. Int. J. Photoenergy **7,** 1–9 (2005).

19. B. Vijayan, N.M. Dimitrijevic, T. Rajh, K. Gray, Effect of calcination temperature on the photocatalytic reduction and oxidation processes of hydrothermally synthesized titania nanotubes. J. Phys. Chem. C. **114,** 12994–13002 (2010).

20. S. Mozia, E. Borowiak-Paleń, J. Przepiórski, B. Grzmil, T. Tsumura, M. Toyoda, J. Grzechulska-Damszel, A.W. Morawski, Physico-chemical properties and possible

photocatalytic applications of titanate nanotubes synthesized via hydrothermal method. J. Phys. Chem. Solids. **71,** 263–272 (2010).

21. W.F. Zhang, Y.L. He, M.S. Zhang, Z. Yin, Q. Chen, Raman scattering study on anatase TiO_2 nanocrystals. J. Phys. D. Appl. Phys. **33,** 912–916 (2000).

22. T. Beuvier, M. Richard-Plouet, L. Brohan, Accurate methods for quantifying the relative ratio of anatase and TiO_2(B) nanoparticles. J. Phys. Chem. C. **113,** 13703–13706 (2009).

23. M. Meksi, A. Turki, H. Kochkar, L. Bousselmi, C. Guillard, G. Berhault, The role of lanthanum in the enhancement of photocatalytic properties of TiO_2 nanomaterials obtained by calcination of hydrogenotitanate nanotubes. Appl. Catal. B Environ. **181,** 651–660 (2016).

24. J.W. Ma, W. Li, N.T. Le, J.A. Diaz-Real, M. Body, C. Legein, J. Swiatowska, A. Demortière, O.J. Borkiewicz, E.A. Konstantinova, A.I. Kokorin, N. Alonso-Vante, C. Laberty-Robert, D. Dambournet, Red-Shifted Absorptions of Cation-Defective and Surface-Functionalized Anatase with Enhanced Photoelectrochemical Properties. ACS Omega **4,** 10929-10938 (2019).

25. A.M. Pennington, A.I. Okonmah, D.T. Munoz, G. Tsilomelekis, F.E. Celik, Changes in Polymorph Composition in P25-TiO_2 during Pretreatment Analyzed by Differential Diffuse Reflectance Spectral Analysis. J. Phys. Chem. C **122,** 5093-5104 (2018).

26. N. Murakami, T.A. Kamai, T. Tsubota, T. Ohno, Control of the crystal structure of titanium(IV) oxide by hydrothermal treatment of a titanate nanotube under acidic conditions. CrystEngComm. **12,** 532–537 (2010).

27. I. Abdouli, F. Dappozze, M. Eternot, C. Guillard, N. Essayem, TiO_2 Catalyzed Dihydroxyacetone (DHA) Conversion in Water: Evidence That This Model Reaction Probes Basicity in Addition to Acidity. Molecules **27,** 8172 (2022).

28. I. Singh, B. Birajdar, Synthesis, characterization and photocatalytic activity of mesoporous Na-doped TiO_2 nano-powder prepared via a solvent-controlled non-aqueous sol-gel route, RSC Adv. **7,** 54053–54062 (2017).

29. N.T. Sahrin, R. Nawaz, F.K. Chong, S.L. Lee, M.D.H. Wirzal, Current perspectives of anodized TiO_2 nanotubes towards photodegradation of formaldehyde: A short review, Environ. Technol. Innov. **22,** 101418 (2021).

30. T. Zhang, B. Yu, D. Wang, F. Zhou, Molybdenum-doped and anatase/rutile mixed-phase TiO2 nanotube photoelectrode for high photoelectrochemical performance. J. Power Sources. **281,** 411–416 (2015).

Author Contributions

GB: conceptualization, ZR, FD and GB: methodology, CG and GB: validation, formal analysis, ZR, GB and CG: investigation, FD: resources, ZR: writing – original draft presentation, GB: writing – review and editing, CG and GB: supervision, GB: project administration, ZR and GB: funding acquisition. All authors have read and agreed to the published version of the manuscript.

Funding

Funding was provided by Campus France (Grant No. 971239J) and Région Auvergne-Rhône-Alpes.

Data Availability Statement

The authors declare that the data supporting the findings of this study are available within the paper and its Supplementary Information file. Should any raw data files be needed in another format they are available from the corresponding author upon reasonable request.

Table 1. A summary of the experimental conditions used to prepare the TiO_2 nanotubes with their corresponding specific surface areas (SSA), their sodium amount as determined by ICP-OES and their anatase crystallite size (XRD).

Sample	**pH after neutralization**	**Residence Time with NaOH (h)**	**Temperature for the washing steps (°C)**	**Rate for the washing steps**	**SSA (m^2/g)**	**Na amount (wt%)**	**Anatase crystallite cize (nm)**
1	6.6	18	60	High	210	< 200 ppm	9.1
2	6.6	18	60	High	200	0.01	9.2
3	6.7	18	60	High	211	0.01	9.2
4	6.7	18	60	High	226	0.02	8.7
5	6.6	18	60	High	213	0.01	8.7
6	6.7	18	60	High	205	0.01	9.0
7	6.8	18	60	Low	160	0.01	11.8
8	6.7	18	80	High	285	0.01	6.5
9	6.7	24	60	High	253	0.01	8.0

Table 2. Initial degradation rates, conversion after 10 min of reaction and time necessary for achieving full conversion for the different TiO_2 samples with BET surface areas ranging between 160 and 285 m^2/g.

Preparation	**S_{BET} (m^2/g)**	**r_0 ($\mu mol.L^{-1}$)**	**Conversion after 10 min (%)**	**Time for 100% conversion (min)**
1	160	50.8	51	21
2	200	62.3	64	16
3	205	61.2	63	17
4	210	59.7	63	17
5	211	62.9	65	16
6	213	61.2	63	17
7	226	59.5	63	17
8	253	47.7	53	21
9	285	28.6	32	36

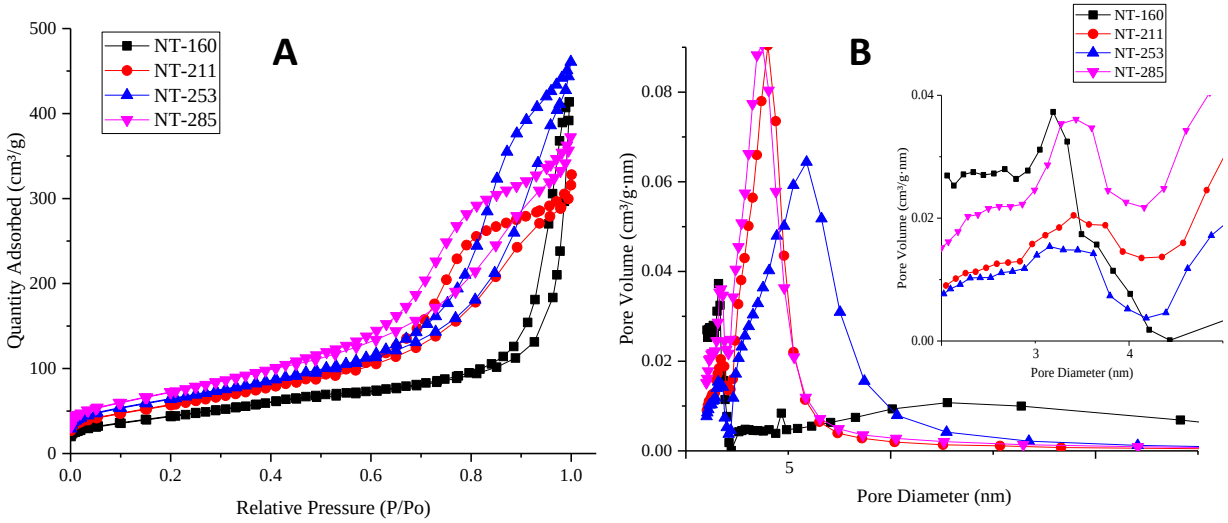

Figure 1. A) N_2 adsorption-desorption isotherms and B) BJH pore size distributions of the most representative TiO_2 samples with S_{BET} values of 160, 211, 253, and 285 m^2/g. The inset in B is a zoom on the region corresponding to pore sizes below 5 nm.

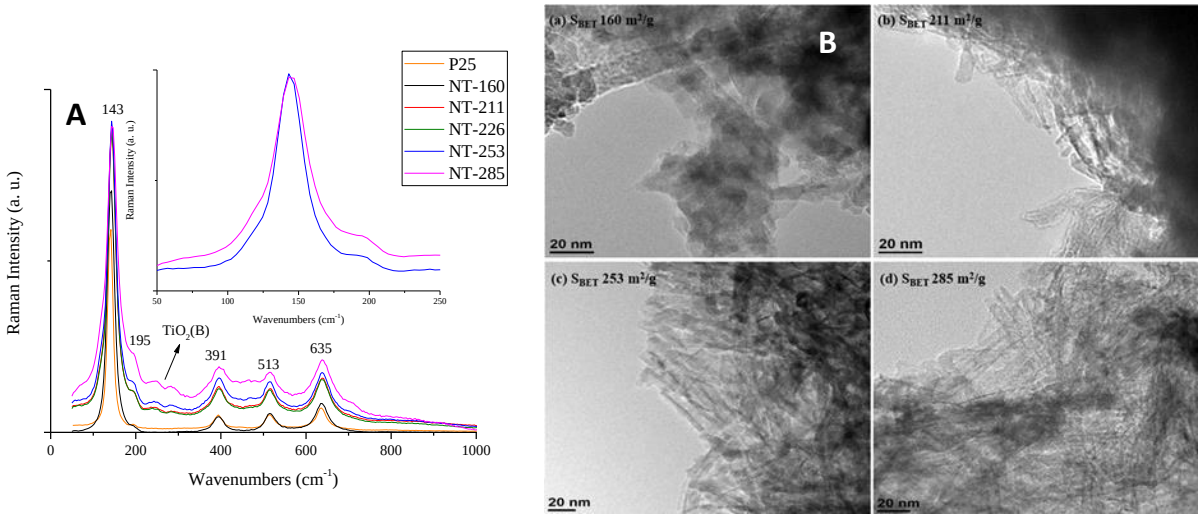

Figure 2. A) Raman spectra of the prepared TiO_2 samples exhibiting various BET specific surface areas. Main vibrational bands due to the anatase phase are indicated on the figure. B) TEM images of nanotubes for the most representative samples with BET specific surface areas of (a) 160, (b) 211, (c) 253, and (d) 285 m^2/g.

Graphical Abstract